Rhythmic pore dynamics in a shrinking lipid vesicle

Tsutomu Hamada,[1,*] Yuichi Hirabayashi,[1] Takao Ohta,[2] and Masahiro Takagi[1]
[1]*School of Materials Science, Japan Advanced Institute of Science and Technology, 1-1 Asahidai, Nomi, Ishikawa 923-1292, Japan*
[2]*Department of Physics, Graduate School of Science, Kyoto University, Kyoto 606-8502, Japan*
(Received 27 August 2009; revised manuscript received 25 October 2009; published 24 November 2009)

The rhythmic motion of membrane pore behavior under nonequilibrium conditions was studied. Application of the surfactant triton X-100 (TX-100) caused lipid vesicles to exhibit two types of shrinking dynamics with pore generation, which depended on both the size of the vesicles and the concentration of added TX-100. Small vesicles and the addition of a low concentration of TX-100 resulted in rhythmic-pore dynamics, where a transient pore was generated within a vesicle in a repetitive manner. In contrast, large vesicles and a high concentration of TX-100 led to continuous-pore dynamics, where the vesicle maintained an open pore during the shrinking process. In the rhythmic-pore membrane, long-cycle oscillation was observed with large vesicles and a low concentration TX-100. The period of one cycle decreased with a decrease in the vesicle size and an increase in the TX-100 concentration. We discuss the mechanism of these trends by considering the elastic free energy of the membrane.

DOI: 10.1103/PhysRevE.80.051921 PACS number(s): 87.16.D−, 82.70.Uv, 05.70.Np

I. INTRODUCTION

It is important to understand the physical mechanisms that govern the dynamical motions and properties of cell plasma membranes [1]. Giant lipid vesicles have been studied as a simple model of biological membranes [2–4]. Giant vesicles with a diameter on the order of 10 μm are large enough to allow the direct real-time microscopic observations of membrane dynamics at the level of single vesicles. Many experimental studies using giant vesicles have been conducted to analyze the stable membrane structure and/or its changes upon exposure to external stimuli [2,4–13]. Theoretical studies have also been used to develop models in terms of elastic bending energies [14–19]. These models have been able to predict several vesicular morphologies, including prolate, oblate, stomatocyte, and bud, that are indeed observed by optical microscopy [20,21]. Thus, the equilibrium mechanical properties of vesicles are relatively well understood. Recently, the dynamical behaviors of nonequilibrium membranes have attracted considerable attention [22] (e.g., rhythmic membrane shrinkage induced by chemical reactions [23–27], enhanced membrane fluctuation due to the activity of embedded ion pumps [28–31], and the dynamics of vesicles in shear flow [32–40].)

Rhythmic motion with energy dissipation is a typical phenomenon under nonequilibrium conditions. If we can reveal the mechanism that underlies rhythmic events in lipid membranes, we should be able to reach a better understanding of the biophysical properties of microscale membrane systems that are out of equilibrium, such as living cells. Nomura *et al.* reported the rhythmic (stepwise) membrane shrinkage of giant vesicles upon exposure to surfactants [23]. It has also been reported that the solubilization of lipid bilayers by surfactants is accompanied by morphological changes in the bilayer and the emergence of mixed micelles [41], which facilitates the extraction of membrane proteins from biomembranes. The presumed steps in the process of the solubilization are as follows: the incorporation of surfactants into membranes leads to an increase in vesicular size until the bilayers are saturated with surfactants and then the saturated membranes shrink to form lipid-surfactant mixed micelles [42–45]. Nomura *et al.* observed the dynamic aspects of the solubilization of giant lipid vesicles by surfactants using dark-field microscopy and found that vesicles exposed to various surfactants exhibited unusual behaviors, such as rhythmic shrinkage, inside-out inversion, opening-up, and bursting [23]. A variety of transformations depended on the combinations of the membrane materials and added surfactants. In rhythmic shrinkage, vesicles show intermittent tremors in membrane fluctuation and a stepwise decrease in size. The interval between tremors decreased as the liposomal size decreased. Theories have been developed to explain such membrane dynamics. Umeda *et al.* performed a Fourier analysis of the membrane fluctuation dynamics [46]. Kaga *et al.* formulated kinetic equations of the stepwise shrinkage dynamics by assuming that it consists of two processes [47,48]: the nucleation process of a pore under an increase in membrane tension and closure of the pore due to the line tension of the pore edge after the leakage of inner fluid. However, in contrast to this progress in theoretical studies, there have been no further experimental studies on surfactant-induced rhythmic events in a membrane system.

In this paper, we obtained real-time observations and performed a systematic analysis of the rhythmic shrinkage of giant lipid vesicles interacting with surfactant molecules. We chose the zwitterionic lipid dioleoyl *L*-α phosphatidylcholine (DOPC) as the membrane material and the nonionic surfactant triton X-100 (TX-100) since this combination readily reproduces the previously reported rhythmic behavior [23]. We found that lipid vesicles exhibit two types of shrinking dynamics with pore generation: rhythmic-pore and continuous-pore dynamics. Each of these are observed depending on both the size of the vesicles and the concentration of added TX-100. We theoretically discuss the mechanism of this difference in the dynamics of membrane shrinking by considering the elastic free energy of bilayer membranes.

*Author to whom correspondence should be addressed; t-hamada@jaist.ac.jp; http://www.jaist.ac.jp/~t-hamada/index.html

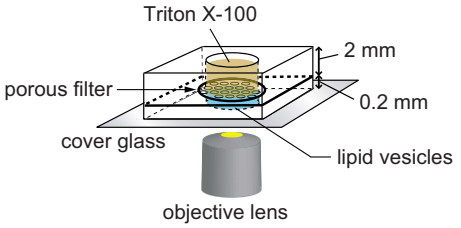

FIG. 1. (Color online) Schematic illustration of an observation chamber that permits the gradual interaction of lipid vesicles and TX-100.

II. EXPERIMENTS

DOPC was obtained from avanti polar lipids. The fluorescent lipid *N*-(rhodamine red-X)-1,2-dihexadecanoyl-sn-glycero-3-phosphoethanolamine triethylammonium salt (rhodamine-PE) was obtained from invitrogen. TX-100 and *D*(+)-glucose were purchased from Nacalai Tesque. Giant vesicles were prepared from dry lipid films of DOPC by the natural swelling method. Briefly, the lipid was dissolved in chloroform/methanol (2:1, v/v) along with rhodamine-PE and *D*(+)-glucose ([lipid]/[glucose]=1:3 molar ratio) in a glass test tube and dried under vacuum for 3 h to form thin lipid films [49]. The tube was placed in a desiccator for 3 h to remove the organic solvent. The film was then swollen with distilled water for 15 h at 37 °C. The final concentrations were 0.05 mM DOPC and 2 mol% rhodamine-PE. We constructed an observation chamber with two compartments separated by a porous filter (pore diameter 0.2 μm, Whatman) (Fig. 1). The vesicle solution (6 μL) was placed in the lower compartment, and 40 μL of suitably diluted TX-100 solution was added to the upper compartment. The vesicles were then allowed to gently interact with the added TX-100 molecules [9]. Time-dependent changes in membrane morphology were observed using a fluorescent microscope (IX71, Olympus) equipped with a confocal scanner (CSU-10, Yokogawa), and the images were recorded on HDD at 30 frame/s.

III. RESULTS

Our observation chamber enabled us to follow the entire process of the dynamic response of lipid vesicles after the application of external stimuli. We first chose a single vesicle with a spherical structure and then added surfactant solution to the chamber to start the stimulation. Observation continued until the vesicles dissolved and disappeared or for several tens of minutes, which was the time limit for the photobleaching of the fluorescent dye. Upon treatment with TX-100, lipid vesicles exhibit deformation dynamics prior to the membrane shrinkage reported by Nomura *et al.* [23] [Fig. 2(a)]. After the introduction of TX-100, thin membrane tubes appeared in the spherical vesicle, and the fluctuation of the vesicular membrane was enhanced. The tubes gradually became thicker and were absorbed by the largely convoluted membrane surface. Once the vesicle was fully deformed, membrane fluctuation gradually decreased until a completely spherical structure was achieved. Careful observations confirmed that the membrane area gradually increased and then decreased during vesicular deformation. Thus, TX-100 led to an episodic increase in vesicle size followed by membrane shrinkage. The diameter of the reformed spherical vesicle was almost equal to the initial diameter before interaction with TX-100 [Fig. 2(b)]. The essentially equal diameters of the spherical vesicles before and after deformation suggest that the area of the membrane surface changes with an almost constant vesicular volume during transformation, as shown in Fig. 2(a). Therefore, upon treatment with TX-100, the membrane area undergoes an episodic increase while the volume remains constant. Then, the amount of membrane materials decreases, and the area returns to its original value. Even after shrinkage into a spherical shape, disintegration of the membrane by surfactant molecules proceeded. As a result, the vesicle membrane material became increasingly insufficient to encapsulate the enclosed incompressible aqueous volume, which led to pore generation within the bilayer membrane (pore-shrinking dynamics, Fig. 3).

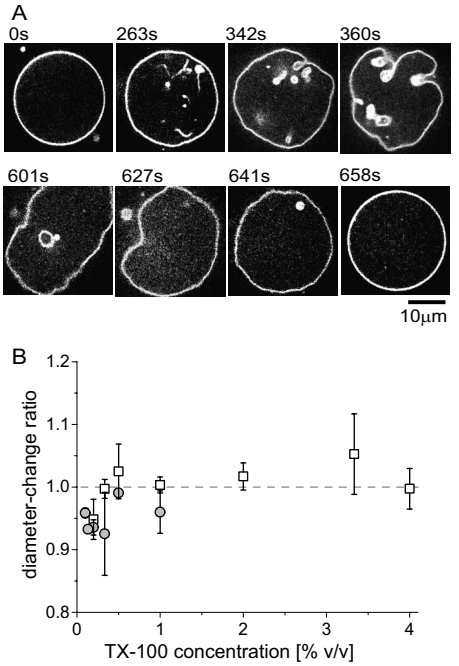

FIG. 2. (a) Vesicular deformation prior to the formation of a membrane pore under treatment with TX-100. Time elapsed after the addition of TX-100 to the vesicles. (b) Diameter-change ratio (diameter of spherical vesicles after deformation divided by that before deformation) at different TX-100 concentrations. The shaded circles and open squares represent vesicles that went on to show rhythmic-pore and continuous-pore dynamics after the temporary behavior shown in Fig. 2(a), respectively.

We found that there are two distinct membrane pore dynamics in the shrinkage process: either a transient pore was generated in a repetitive manner [Fig. 3(a), rhythmic-pore shrinkage] or an open pore remained in a vesicular membrane until the vesicle became smaller and disappeared at the microscopic level [Fig. 3(b), continuous-pore shrinkage]. Notably, we never observed multiple pores in a vesicular membrane under our experimental conditions. Membrane thermal fluctuation can be observed only during the period of

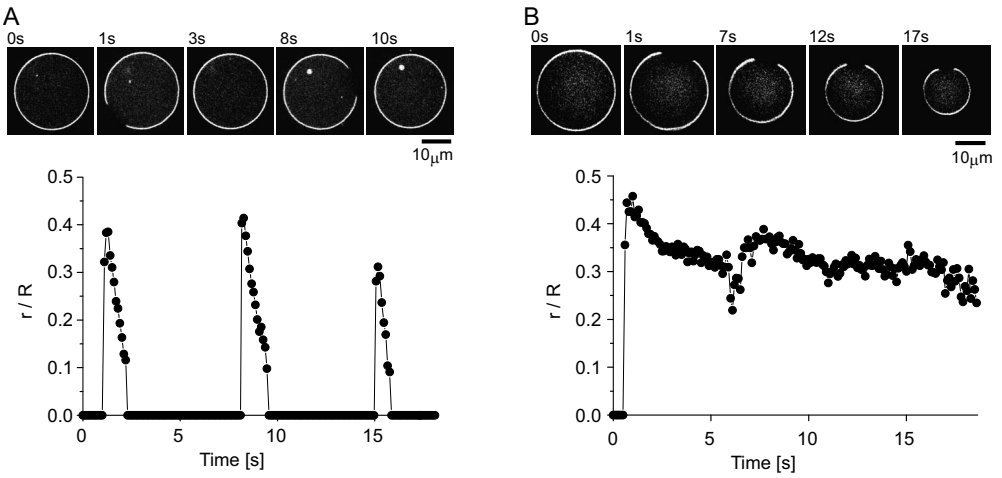

FIG. 3. Microscopic image sequences of membrane pore dynamics in shrinking vesicles under treatment with TX-100. (a) Rhythmic-pore shrinkage, where a transient pore was generated in a repetitive manner. Also see a movie in [50]. (b) Continuous-pore shrinkage, where a pore remained intact during the shrinkage process. Also see a movie in [50]. Time traces of the pore radius r divided by the vesicle radius R are shown at the bottom of each image. Time zero is chosen as the point at which a sphere was achieved after the deformation of a vesicle as shown in Fig. 2(a).

pore opening as theoretically predicted [46]. From cross-sectional images of vesicles, we measured the time trace of the pore radius r divided by the vesicle radius R in the two shrinkage processes. In rhythmic-pore shrinkage, the vesicle exhibited periodic oscillatory pore formation [Fig. 3(a)]. In a single cycle, a pore opens rapidly to reach its largest size, and then gradually closes. The duration of pore opening is much shorter than the time with no hole. Successive pores were generated at apparently random locations [51]. In contrast, in continuous-pore shrinkage, the vesicle maintained an open pore during shrinkage [Fig. 3(b)]. The temporal fluctuation of r/R as measured from cross-sectional images can be attributed to the out-of-focus position of the pore due to thermal rotation of the vesicle. The rate of the decrease in vesicle size dR/dt in rhythmic-pore shrinkage was slower than that in continuous-pore shrinkage.

Next, we analyzed the periodic oscillatory behavior of rhythmic-pore membranes. Figure 4(a) shows the cycle period of rhythmic-pore motion for a vesicle as a function of the vesicle diameter; the period of a cycle decreased with a decrease in vesicle size. This trend is in good agreement with the observations of Nomura *et al.* [23]. The relation between the cycle period and the TX-100 concentration for vesicles with a diameter of 15 μm is shown in Fig. 4(b). A high concentration of TX-100 produced a rhythmic-pore with a short cycle. Thus, both the vesicle size and concentration of added TX-100 affect the oscillatory cycle for a rhythmic-pore membrane.

As shown in Fig. 3, a shrinking vesicle shows two distinct membrane pore behaviors: rhythmic and continuous changes. We examined the probability of the two membrane pore motions as a function of the concentration of added TX-100 from 0.1 to 4%v/v [Fig. 5(a)]. At low concentrations of TX-100, most vesicles exhibit rhythmic-pore shrinkage, while at high concentrations of TX-100 vesicles tend to undergo continuous-pore shrinkage. Moreover, Fig. 5(b) shows the size distributions of rhythmic- and continuous-pore shrinking vesicles under treatment with 0.2%, 1%, and 4% TX-100, where the vesicle size was measured just before the first pore opened. There is a clear trend in the appearance of the two pore dynamics. The histogram of 1% TX-100 indicates that larger vesicles tend to exhibit continuous-pore dynamics, while smaller vesicles show rhythmic-pore dynamics. In addition, Fig. 5(c) shows the average diameter of vesicles undergoing rhythmic- and continuous- pore dynamics at each

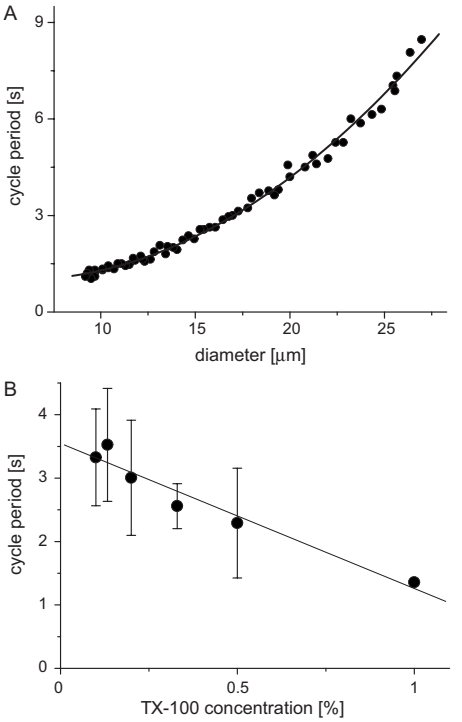

FIG. 4. Periodic oscillatory motion of rhythmic-pore shrinkage. (a) Cycle period as a function of the diameter of a single vesicle with 0.2% TX-100. (b) Cycle period as a function of the TX-100 concentration for vesicles with a diameter of 15 μm.

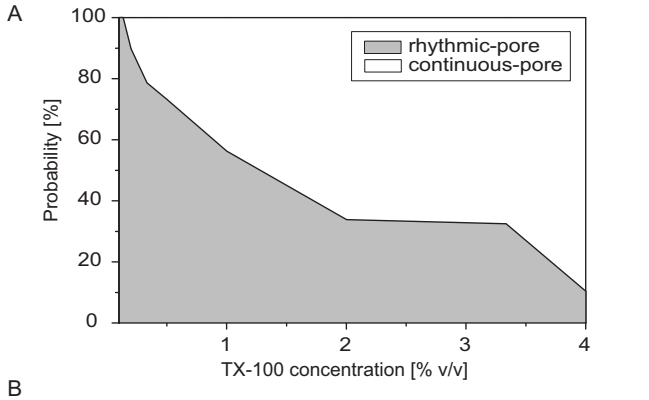

C

TX-100 concentration	0.2%	0.33%	0.5%	1%	2%	3.3%	4%
continuous-pore d_{av} [μm]	20.9	27.1	21.5	20.2	18.5	16.6	19.2
rhythmic-pore d_{av} [μm]	18.9	18.0	14.4	11.3	11.9	10.2	12.2

FIG. 5. (a) Probability of rhythmic-pore and continuous-pore dynamics as a function of the TX-100 concentration. The number of vesicles observed for each surfactant concentration are $n=29$ (4% TX-100), 77 (3.3% TX-100), 74 (2% TX-100), 80 (1% TX-100), 67 (0.5% TX-100), 70 (0.33% TX-100), 39 (0.2% TX-100), 13 (0.13% TX-100), and 8 (0.1% TX-100). (b) Size distributions of rhythmic- (shaded bar) and continuous-pore (open bar) shrinking vesicles at 0.2%, 1%, and 4% TX-100. The black solid and dashed lines are Gaussian fits to the data of rhythmic- and continuous-pore dynamics, respectively. The gray solid line shows the size distribution of total vesicles independent of pore behavior. (c) Average diameters (d_{av}) of vesicles that exhibit rhythmic- and continuous-pore shrinkage under each TX-100 concentration. The diameter was measured just before formation of the first pore.

TX-100 concentration. At any concentration of TX-100, vesicles with continuous-pore dynamics are larger than those with rhythmic-pore dynamics. Therefore, the size of vesicles is the main parameter that determines the difference in the two pore dynamics, and the critical vesicle size depends on the TX-100 concentration.

Additionally, we rarely observed a vesicle that underwent a transition from continuous- to rhythmic-pore motion. Figure 6 shows microscopic image sequences of such a change in pore dynamics. A vesicle undergoing continuous-pore motion suddenly closed its pore and then exhibited rhythmic-pore shrinkage. The reverse transition, from rhythmic- to continuous-pore, was never observed. This behavior of a single vesicle is associated with the statistical trend shown in Fig. 5: a larger vesicle exhibits continuous-pore motion, while a smaller vesicle shows rhythmic-pore motion.

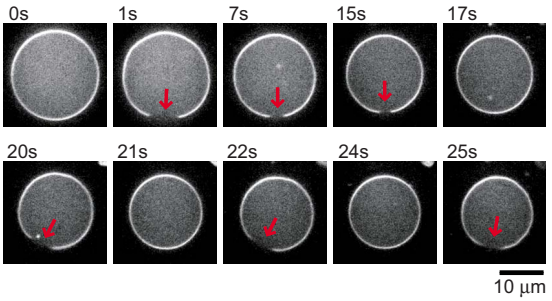

FIG. 6. (Color online) Microscopic image sequence of the transition from continuous- to rhythmic-pore shrinking dynamics in a single vesicle. Arrows represent the pore that has opened within the membrane.

IV. DISCUSSION

The present results show that the application of TX-100 caused lipid vesicles to exhibit two types of shrinking dynamics with pore generation, which depend both on the size of the vesicles and the concentration of added TX-100. A qualitative phase diagram of the membrane pore dynamics is shown in Fig. 7 for vesicle size and the TX-100 concentration. As shown in Fig. 5, small vesicles and the addition of a low concentration of TX-100 result in rhythmic-pore dynamics, while large vesicles and a high concentration of TX-100 lead to continuous-pore dynamics. Additionally, at the rhythmic-pore membrane, large vesicles and a low concentration of TX-100 produce long-cycle oscillation; the cycle period decreased with a decrease in the vesicle size and an increase in the TX-100 concentration (Fig. 4).

We now discuss the mechanism of this trend in membrane-shrinking dynamics by considering the elastic free energy of lipid vesicles. Let us consider a spherical vesicle with radius R which can have only one circular pore with radius r. When a pore exists in the vesicle membrane, the vesicle surface area is given by $4\pi R^2-\pi r^2=S-\pi r^2$, where S is the surface area of a sphere with radius R. We set $r=0$ when there is no pore in the vesicle. An important basic quantity of a vesicle membrane is the equilibrium area a, which is the optimal surface area per lipid molecule on the vesicle surface. When the total number of lipid molecules in one layer of the vesicle is N, the total equilibrium area A is given by $A=aN$. In the present problem, N is a decreasing

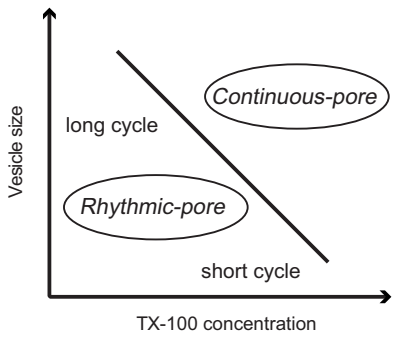

FIG. 7. Phase diagram of the membrane pore dynamics in shrinking vesicles.

function of time because the lipid molecules are pulled away from the vesicle surface by the formation of mixed micelles with surfactant molecules contained in the surrounding solutions [52]. Therefore, the actual surface area of the vesicle differs from the optimal area as disintegration proceeds provided that the vesicle radius is time independent when no pore is open.

The time-evolution equations for the pore radius r, the total surface of the vesicle $S=4\pi R^2$, and the optimal surface A are given by [47]

$$r\dot{r} = -\frac{\pi\gamma\ell}{\zeta}\left(\frac{\pi r^4}{A^2} - \frac{\sigma r^2}{\gamma\ell} + \frac{r}{\ell}\right) = -\frac{\pi\gamma\ell}{\zeta}\left(\frac{\pi r^4}{A^2} - \frac{(S-A)r^2}{A^2} + \frac{r}{\ell}\right), \tag{1}$$

$$4\pi R\frac{dR}{dt} = \frac{dS}{dt} = -\frac{8\pi C}{3\eta S}\frac{(S-A-\pi r^2)}{A^2}r^3, \tag{2}$$

$$\frac{dA}{dt} = -\alpha A, \tag{3}$$

where ζ is the surface viscosity, η is the viscosity of the internal water, and γ is the line tension of the pore. The constant C is given by [25]

$$C = \frac{192\pi^2\kappa^2}{k_B T}, \tag{4}$$

where κ is the bending modulus, k_B is the Boltzmann constant, and T is the absolute temperature. The characteristic length ℓ is defined by

$$\ell = \frac{C}{\gamma}. \tag{5}$$

The membrane tension σ is given by

$$\sigma = C\frac{S-A}{A^2}. \tag{6}$$

When σ is sufficiently large, there are two solutions of Eq. (1) for $r>0$; i.e., $r=r_c$ and $r=r_s(>r_c)$, where r_c is the location of the local maximum in the free energy and r_s is at the absolute minimum of the free energy. During the shrinking dynamics, lipid molecules are pulled away from the vesicle by surfactants, which leads to a decrease in A as in Eq. (3). Thus, the increased membrane tension σ triggers the nucleation of a pore with radius r: the absolute minimum of the free energy appears at a finite value of r. After the formation of a pore by nucleation, the internal water can leak out through the pore and S decreases. Assuming $A=$const, Kaga and Ohta performed numerical simulations of the pore closing dynamics for rhythmic-pore membranes [47]. However, our microscopic observations revealed that vesicles exhibit not only rhythmic-pore behavior but also continuous-pore behavior, where the membrane pore remains open during shrinkage. Here, based on the model presented by Kaga and Ohta [47], we discuss the observed trend in the two membrane pore dynamics by considering the changes in both A and S.

Since Eq. (1) has a stable steady solution for fixed A and S, we set $dr/dt=0$:

$$\pi r^2 - (S-A) = -\frac{A^2}{r\ell}. \tag{7}$$

By substituting this into Eq. (2), we have

$$\frac{dS}{dt} = -\frac{8\pi C}{3\eta\ell}\frac{r^2}{S}. \tag{8}$$

If $A \ll r\ell$, the solution of Eq. (7) can be approximated as $\pi r^2 \approx S-A$ and hence

$$\frac{dS}{dt} = -\frac{8C}{3\eta\ell}\frac{S-A}{S}. \tag{9}$$

From Eqs. (3) and (9), we obtain the ratio of the rates of changes in the actual and optimal surface areas

$$Q \equiv \frac{dS}{dt}/\frac{dA}{dt} = \frac{8\gamma}{3\alpha\eta}\frac{1-A/S}{A}. \tag{10}$$

Since α is proportional to the surfactant concentration C_{surf}, i.e., $\alpha=\alpha' C_{surf}$, the condition for which $Q\sim 1$ is thus found to be

$$\frac{8\gamma}{3\alpha'\eta} \sim AC_{surf}, \tag{11}$$

where we have assumed, for simplicity, $A \ll S$. When the ratio Q of the dynamics of S and A is large, A is very slow so that S catches up A, indicating that the membrane tension σ drops and the pore is closed. After a while, a new pore is nucleated and the process is repeated as a rhythmic shrinkage. On the other hand, when the ratio Q is small, the difference $S-A$ may not become zero. In this case, the pore remains open and the shrinkage is continuous. Thus, when the vesicle is large (A and S are large but keeping $A \ll S$) and the surfactant concentration is high, Q is small and hence continuous shrinkage is expected. In contrast, when the vesicle is small and the surfactant concentration is low, the time variation in A is slow and hence rhythmic shrinkage is expected. Thus, our model explains the observed trend in the membrane pore dynamics as shown in Fig. 7.

The oscillatory tendency of rhythmic-pore dynamics with regard to vesicle size and TX-100 concentration can also be explained in terms of the elastic free energy. Since the duration of the no-pore state is much longer than that of the pore-opening state in a given cycle [Fig. 3(a)], most of a cycle period is spent waiting for nucleation in pore formation. If the concentration of TX-100 is high, the decrease in A (increase in σ) is fast. In this situation, the waiting time (no-pore period) is very short. Thus, a large amount of TX-100 should induce rhythmic-pore dynamics with a short cycle. In addition, it has also been deduced that the period of one cycle is proportional to the square of the vesicle radius [47].

Real-time microscopic observations revealed the whole dynamical process of lipid vesicles in surfactant-induced membrane solubilization. We found that the vesicle acquires

a temporary increase in excess membrane area that allows large vesicular deformations, as shown in Fig. 1, before the shrinking dynamics [53]. The first membrane-expansion behavior was observed independent of the subsequent rhythmic- and continuous-pore dynamics. In a report on the surfactant solubilization of submicron large unilamellar vesicles (LUVs), a three-stage model was proposed [42–45]. First, the incorporation of surfactants into membranes leads to an increase in vesicular size. Second, the saturated membranes disintegrate because of the formation of lipid-surfactant mixed micelles. Finally, all of the membrane material is converted into mixed micelles. Thus, TX-100 first leads to an increase in surface area by becoming incorporated into the bilayer membrane, and this is followed by a decrease in area. This previous study using submicron vesicles supports our results obtained with μm-sized giant vesicles.

In summary, we studied the oscillatory pore motion of fluid vesicles in a membrane solubilization process. Microscopic observations clarified the dynamic phase diagram of shrinking vesicles as a function of vesicle size and the concentration of surfactant. Rhythmic-pore dynamics can appear with smaller vesicles and a lower concentration of the surfactant. The cycle period decreased with a decrease in the vesicle size and an increase in the TX-100 concentration. These trends can be explained in terms of the time-dependent change in membrane tension as deduced from the elastic free energy. These findings may contribute to a better understanding of nonequilibrium membrane mechanics.

ACKNOWLEDGMENTS

Technical advice and assistance from Dr. Fumimasa Nomura, Dr. Takehiko Inaba, and Dr. Sumiko Araki is greatly appreciated. We thank Dr. Mun'delanji Vestergaard for critically reading the paper. This work was supported by a KAKENHI Grant-in-Aid for Scientific Research (B) (Grant No. 20360370) from the Japan Society for the Promotion of Science (JSPS) and on Priority Areas "Soft Matter Physics" and "Bio Manipulation" from the Ministry of Education, Culture, Sports, Science, and Technology (MEXT) of Japan.

[1] R. Lipowsky and E. Sackmann, *Structure and Dynamics of Membranes* (Elsevier, New York, 1995).
[2] P. L. Luisi and P. Walde, *Giant Vesicles* (Wiley & Sons, New York, 2000).
[3] H.-G. Döbereiner, Curr. Opin. Colloid Interface Sci. **5**, 256 (2000).
[4] R. Dimova, S. Aranda, N. Bezlyepkina, V. Nikolov, K. A. Riske, and R. Lipowsky, J. Phys.: Condens. Matter **18**, S1151 (2006).
[5] A. Karlsson, R. Karlsson, M. Karsson, A.-S. Cans, A. Strömberg, F. Ryttsén, and O. Orwar, Nature (London) **409**, 150 (2001).
[6] I. Tsafrir, Y. Caspi, M.-A. Guedeau-Boudeville, T. Arzi, and J. Stavans, Phys. Rev. Lett. **91**, 138102 (2003).
[7] R. Bar-Ziv, E. Moses, and P. Nelson, Biophys. J. **75**, 294 (1998).
[8] T. Baumgart, S. T. Hess, and W. W. Webb, Nature (London) **425**, 821 (2003).
[9] T. Hamada, Y. Miura, K. Ishii, S. Araki, K. Yoshikawa, M. Vestergaard, and M. Takagi, J. Phys. Chem. B **111**, 10853 (2007).
[10] N. Khalifat, N. Puff, S. Bonneau, J.-B. Fournier, and M. I. Angelova, Biophys. J. **95**, 4924 (2008).
[11] S. L. Veatch and S. L. Keller, Biochim. Biophys. Acta **1746**, 172 (2005).
[12] E. Evans, V. Heinrich, F. Ludwig, and W. Rawicz, Biophys. J. **85**, 2342 (2003).
[13] M. Yanagisawa, M. Imai, and T. Taniguchi, Phys. Rev. Lett. **100**, 148102 (2008).
[14] U. Seifert, K. Berndl, and R. Lipowsky, Phys. Rev. A **44**, 1182 (1991).
[15] L. Miao, U. Seifert, M. Wortis, and H.-G. Döbereiner, Phys. Rev. E **49**, 5389 (1994).
[16] U. Seifert, Adv. Phys. **46**, 13 (1997).
[17] P. Ziherl and S. Svetina, Europhys. Lett. **70**, 690 (2005).
[18] G. Lim H. W., M. Wortis, and R. Mukhopadhyay, Proc. Natl. Acad. Sci. U.S.A. **99**, 16766 (2002).
[19] L. Bagatolli and P. B. S. Kumar, Soft Matter **5**, 3234 (2009).
[20] J. Käs and E. Sackmann, Biophys. J. **60**, 825 (1991).
[21] K. Ishii, T. Hamada, M. Hatakeyama, R. Sugimoto, T. Nagasaki, and M. Takagi, ChemBioChem **10**, 251 (2009).
[22] S. Ramaswamy and M. Rao, C. R. Acad. Sci., Ser. IV Phys. Astrophys. **2**, 817 (2001).
[23] F. Nomura, M. Nagata, T. Inaba, H. Hiramatsu, H. Hotani, and K. Takiguchi, Proc. Natl. Acad. Sci. U.S.A. **98**, 2340 (2001).
[24] O. Sandre, L. Moreaux, and F. Brochard-Wyart, Proc. Natl. Acad. Sci. U.S.A. **96**, 10591 (1999).
[25] F. Brochard-Wyart, P. G. de Gennes, and O. Sandre, Physica A **278**, 32 (2000).
[26] E. Karatekin, O. Sandre, H. Guitouni, N. Borghi, P.-H. Puech, and F. Brochard-Wyart, Biophys. J. **84**, 1734 (2003).
[27] E. Karatekin, O. Sandre, and F. Brochard-Wyart, Polym. Int. **52**, 486 (2003).
[28] J. Prost and R. Bruinsma, Europhys. Lett. **33**, 321 (1996).
[29] J.-B. Manneville, P. Bassereau, S. Ramaswamy, and J. Prost, Phys. Rev. E **64**, 021908 (2001).
[30] P. Girard, J. Prost, and P. Bassereau, Phys. Rev. Lett. **94**, 088102 (2005).
[31] M. D. El Alaoui Faris, D. Lacoste, J. Pécréaux, J.-F. Joanny, J. Prost, and P. Bassereau, Phys. Rev. Lett. **102**, 038102 (2009).
[32] K. H. de Haas, C. Blom, D. van den Ende, M. H. G. Duits, and J. Mellema, Phys. Rev. E **56**, 7132 (1997).
[33] M.-A. Mader, V. Vitkova, M. Abkarian, A. Viallat, and T. Podgorski, Eur. Phys. J. E **19**, 389 (2006).
[34] J. Deschamps, V. Kantsler, and V. Steinberg, Phys. Rev. Lett. **102**, 118105 (2009).
[35] J. Beaucourt, F. Rioual, T. Séon, T. Biben, and C. Misbah, Phys. Rev. E **69**, 011906 (2004).

[36] H. Noguchi and G. Gompper, Phys. Rev. Lett. **98**, 128103 (2007).
[37] U. Seifert, Eur. Phys. J. B **8**, 405 (1999).
[38] P. M. Vlahovska and R. S. Gracia, Phys. Rev. E **75**, 016313 (2007).
[39] V. V. Lebedev, K. S. Turitsyn, and S. S. Vergeles, Phys. Rev. Lett. **99**, 218101 (2007).
[40] R. Finken, A. Lamura, U. Seifert, and G. Gompper, Eur. Phys. J. E **25**, 309 (2008).
[41] M. Almgren, Biochim. Biophys. Acta **1508**, 146 (2000).
[42] M.-T. Paternostre, M. Roux, and J.-L. Rigaud, Biochemistry **27**, 2668 (1988).
[43] A. de la Maza and J. L. Parra, Langmuir **11**, 2435 (1995).
[44] U. Kragh-Hansen, M. le Maire, and J. V. Møller, Biophys. J. **75**, 2932 (1998).
[45] K.-C. Huang, C.-M. Lin, H.-K. Tsao, and Y.-J. Sheng, J. Chem. Phys. **130**, 245101 (2009).
[46] T. Umeda, F. Nomura, T. Inaba, K. Takiguchi, and H. Hotani, ChemPhysChem **6**, 1047 (2005).
[47] M. Kaga and T. Ohta, Eur. Phys. J. E **21**, 91 (2006).
[48] M. Kaga and T. Ohta, J. Phys. Soc. Jpn. **76**, 094003 (2007).
[49] K. Tsumoto, H. Matsuo, M. Tomita, and T. Yoshimura, Colloids Surf., B **68**, 98 (2009).
[50] See EPAPS Document No. E-PLEEE8-80-119911 for movies of rhythmic-pore shrinkage (movie1.mpeg) and continuous-pore shrinkage (movie2.mpg). The movies shown are in real speed. For more information on EPAPS, see http://www.aip.org/pubservs/epaps.html.
[51] We adjusted the microscopic focus position to the vesicle equator and preferentially detected pores opened at the vesicle equator for the images and movies. In addition to the pores, enhanced membrane thermal fluctuation is observed within the pore-opening vesicles due to the temporary gain of excess area [46]. Even if a pore appears on the pole of vesicles far from the microscopic focus position, we can decide when vesicles open a pore according to the observed membrane fluctuation behavior. Thus, our analyses such as cycle period are not affected by the out-of-focus position of opening pores.
[52] We consider that the loss of membrane materials from the inner and outer leaflets of the bilayer is essentially simultaneous. It is because that surfactant-saturated fluid membranes show rapid flip-flop and materials are quickly distributed between the leaflets, see M. le Maire, J. V. Møller, and P. Champeil, Biochemistry **26**, 4803 (1987).
[53] We previously reported the dynamic response of phase-separated giant vesicles upon the addition of TX-100 in Ref. [9]. The increase in membrane area induced budding of the phase domains due to the line energy of phase boundaries, while the homogeneous vesicles studied here show large deformations of the entire membrane surface.